Li–Se Batteries

DOI: 10.1002/anie.201303147

An Advanced Selenium–Carbon Cathode for Rechargeable Lithium–Selenium Batteries**

*Chun-Peng Yang, Sen Xin, Ya-Xia Yin, Huan Ye, Juan Zhang, and Yu-Guo Guo**

The rapidly developing market for mobile electronics and hybrid electric vehicles (HEVs) has prompted the urgent need for batteries with high energy density, long cycle life, high efficiency, and low cost.[1] Recently, rechargeable lithium-sulfur (Li–S) batteries have attracted considerable attention because of their high theoretical gravimetric (volumetric) energy density of 2570 $Wh\,kg^{-1}$ (2200 $Wh\,L^{-1}$), and low cost.[2] However, the use of S as cathode material for Li–S batteries suffers from two major issues. One is the insulating nature of S, which results in low active-material utilization and limited rate capability.[2a] The other is the formation of electrolyte-soluble polysulfides; these polysulfide intermediates, which are generated in the discharge/charge process, dissolve in the electrolyte and migrate to the Li anode, a process known as the shuttle effect.[3] Consequently, the S cathode suffers a significant loss of S during cycling, resulting in a rapid capacity decrease. Many strategies have been used to address these problems, such as the impregnation of S into various conductive porous matrixes,[4] surface coating of S,[5] and the use of suitable electrolytes[6] and additives.[7] Although remarkable improvements have been achieved, the application of Li–S batteries is still hindered by the intrinsic drawbacks of S. Therefore, it is of great importance to explore and develop new high-energy cathode materials with improved electronic conductivity and cycling stability, to cover the shortfalls of S and provide alternative choices for practical applications.

From this perspective, selenium, an element belonging to the same group in the periodic table as sulfur, is a prospective candidate for cathode materials. Although Se has a lower theoretical gravimetric capacity (675 $mA\,h\,g^{-1}$) than S (1675 $mA\,h\,g^{-1}$), its higher density (ca. 2.5 times that of S) offsets the deficiency and provides a high theoretical volumetric capacity density (3253 $mA\,h\,cm^{-3}$), comparable to that of S (3467 $mA\,h\,cm^{-3}$). It has been reported that Li–Se batteries deliver a high output voltage,[8] so Li–Se batteries are also expected to have a high volumetric energy density. It is known that for applications in portable devices and HEVs, volumetric energy density is more important than gravimetric energy density because of the limited battery packing space.[9] Moreover, the electronic conductivity of Se ($1\times10^{-3}\,S\,m^{-1}$) is considerably higher than that of S ($5\times10^{-28}\,S\,m^{-1}$),[8] which suggests that Se could have higher utilization rate, better electrochemical activity, and faster electrochemical reaction with Li. Therefore, the advantages of Se promise an attractive alternative cathode material for building high-energy batteries for specific applications, including consumer electronics and transportation. However, at present, research on Li–Se batteries is still at a very early stage.

Recently, Abouimrane et al.[8] conducted pioneering work on the use of Se as a cathode material. The results show that, even bulk Se has an active material utilization of ca. 45% upon cycling, which is not commonly observed in Li–S batteries with a bulk S cathode. This suggests that Se cathode has a much better activity and a weaker shuttle effect than S. Nevertheless, bulk Se cannot completely deliver the theoretical capacity. Moreover, given the weak interaction between bulk Se and the conductive substrate, the polyselenide species generated during the Li uptake/release process cannot be effectively restrained on the cathode side. Thus, the shuttle effect of Se is not eliminated, which deteriorates the cycling performance of the Se cathode. To address these issues, encapsulation of Se molecules into a conductive porous carbon matrix may greatly improve the electrochemical performance of Se. However, this assumption has not yet been demonstrated, and the mechanism of the electrochemical reaction between Se molecules and Li remains unclear to date.

Herein, we report a Se composite cathode material, in which Se is confined as cyclic Se_8 molecules in the mesopores of an ordered mesoporous carbon (CMK-3) matrix. When assembled into Li–Se batteries with the water-soluble binder sodium alginate (SA), the Se/CMK-3 composite exhibits novel electrochemical behavior with a single plateau in the discharge/charge process. Data from ex situ Raman and X-ray diffraction (XRD) analysis suggest that this behavior is due to the conversion of cyclic Se_8 molecules into chain-like Se_n molecules in the carbon channels. Given the high electrochemical activity of the chain-like Se_n molecules and the strong interaction between them and the carbon mesopores, this Se cathode shows a high capacity that approaches the theoretical value of Se, and exhibits favorable capacity retention upon cycling.

The Se/CMK-3 composite was synthesized through a facile melt-diffusion process from a ball-milled mixture of

[*] C.-P. Yang, S. Xin, Dr. Y.-X. Yin, H. Ye, J. Zhang, Prof. Y.-G. Guo
CAS Key Laboratory of Molecular Nanostructure and Nanotechnology, and Beijing National Laboratory for Molecular Sciences, Institute of Chemistry, Chinese Academy of Sciences (CAS)
Beijing 100190 (P. R. China)
E-mail: ygguo@iccas.ac.cn

[**] This work was supported by the National Natural Science Foundation of China (51225204, 91127044, and 21121063), the National Basic Research Program of China (2011CB935700, 2009CB930400, and 2012CB932900), and the Chinese Academy of Sciences.

Supporting information for this article, including synthetic methods and structural, electrochemical, and ex situ characterization methods, is available on the WWW under http://dx.doi.org/10.1002/anie.201303147.

CMK-3 (Figure 1a) and Se (Se-CMK-3, Figure 1b). After the heating procedure, all bulk crystalline Se in Se-CMK-3 disappears to yield the Se/CMK-3 composite (Figure 1c). The energy-dispersive X-ray spectroscopy (EDX) spectrum

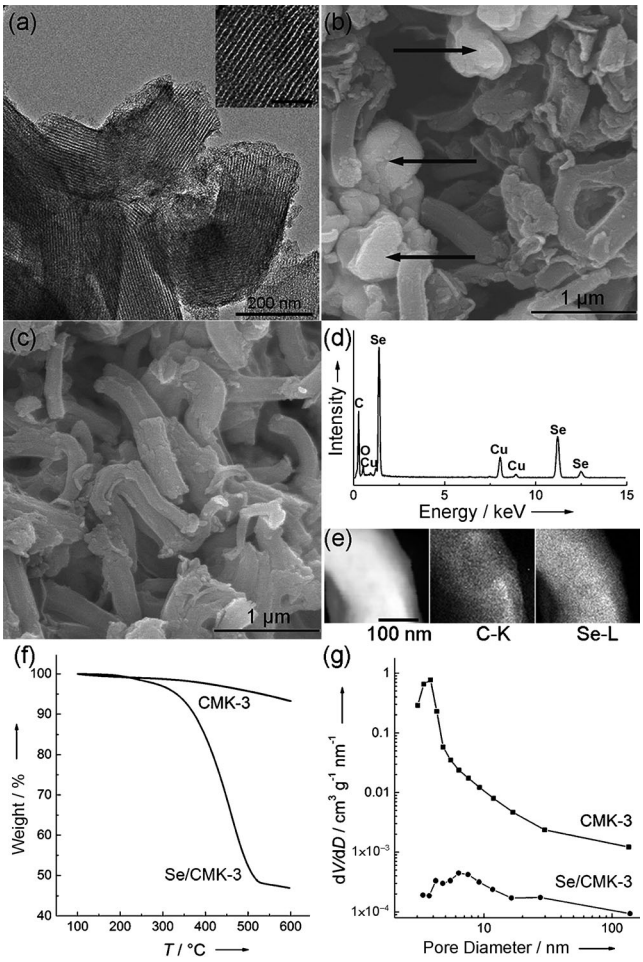

Figure 1. a) TEM image of pristine CMK-3 (inset shows the high-resolution TEM image of CMK-3; scale bar: 50 nm). SEM images of b) Se-CMK-3 and c) Se/CMK-3; the black arrows in (b) indicate bulk Se. d) EDX spectrum of Se/CMK-3. e) Annular dark-field TEM image, and corresponding C and Se elemental mapping of Se/CMK-3. f) TG curves of Se/CMK-3 and CMK-3. g) Pore size distributions of CMK-3 (BET surface area = 1386 $m^2 g^{-1}$, pore volume = 1.276 $cm^3 g^{-1}$) and Se/CMK-3 (BET surface area = 17.2 $m^2 g^{-1}$, pore volume = 0.131 $cm^3 g^{-1}$).

(Figure 1d) of Se/CMK-3 demonstrates the presence of Se, and elemental mapping (Figure 1e) reveals a uniform distribution of Se in CMK-3. The Se content in the composite was determined to be 49.0 wt% by thermogravimetric (TG) analysis (Figure 1f). After Se loading, the Brunauer-Emmett-Teller (BET) surface area and pore volume of CMK-3 decrease markedly, accompanied by a significant reduction in pore size distribution in the mesoporous region (3–4 nm; Figure 1g), which suggests the impregnation of Se into the mesoporous channels of CMK-3. The results agree well with the XRD patterns of the Se-CMK-3 mixture and Se/CMK-3 composite in Figure 2a. All of the diffraction peaks of trigonal Se disappear after heating, which is indicative of good

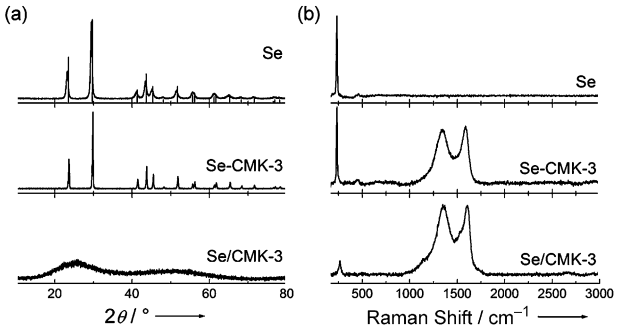

Figure 2. a) XRD patterns and b) Raman spectra of Se, Se-CMK-3, and Se/CMK-3. The drop lines in a) show the XRD patterns of trigonal Se (JCPDS Card No. 06-0362).

dispersion of amorphous Se in CMK-3. To further determine the structure of Se in the composite, the Raman spectra of bulk Se, Se-CMK-3, and Se/CMK-3 were collected and are compared in Figure 2b. Compared with bulk Se, Se-CMK-3 does not show any significant change in Raman shift. After undergoing the Se hosting process, the intensity of the characteristic peak of Se decreases and its position blue shifts, thus suggesting the impregnation of Se into the mesopores of CMK-3 and a possible change in the existing form of Se. These changes will be further discussed below.

Cathodes were prepared from the Se/CMK-3 composite and then paired with Li anodes to assemble Li–Se batteries. A carbonate electrolyte was used, because of its compatibility with the Se cathode.[8] When preparing the Se/CMK-3 cathode, it was found that Se is insoluble in water, but dissolved slightly in *N*-methyl-2-pyrrolidone (NMP; Supporting Information, Figure S1). Therefore, we selected SA, a stable water-soluble binder,[10] as the binder for pasting the Se cathode, to avoid dissolution of Se in NMP. A Se cathode prepared with poly(vinylidene fluoride) (PVDF) binder (dissolved in NMP) was used for comparison.

As illustrated in Figure 3a, with the SA binder the Se/CMK-3 cathode delivers an initial discharge capacity of > 900 (450) mA h g^{-1} (the values outside and inside the parentheses are based on the mass of Se and the mass of the composite, respectively) with a single plateau at ca. 1.90 V. This result is significantly different from that obtained in the previous report.[8] In subsequent cycles, the discharge capacity was approximately 670 (335) mA h g^{-1}, which approaches the theoretical specific capacity of Se (675 mA h g^{-1}). The capacity corresponds to a volumetric capacity density of 2854 (690) mA h cm^{-3} (the values outside and inside the parentheses are based on the density of amorphous Se and the composite, respectively). In subsequent cycles, the discharge/charge processes still behave as a single plateau reaction, but the discharge plateaus are slightly shifted from the first discharge. These results imply that the Se/CMK-3 cathode with SA binder has a high electrochemical activity and a favorable cycling stability. To investigate the irreversible capacity in the first cycle, the electrochemical performance of pristine CMK-3 with SA binder was also tested. As shown in Figure S2, pure CMK-3 displays an irreversible capacity of ca. 300 mA h g^{-1} upon first discharge, which might constitute the

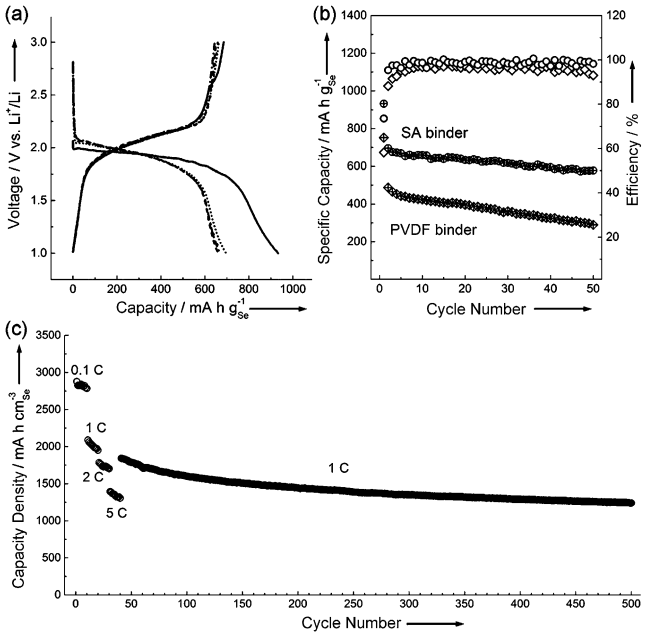

Figure 3. a) Glavanostatic discharge/charge voltage profiles of Se/CMK-3 with SA binder in the voltage range of 1.0–3.0 V (vs. Li^+/Li) at 0.1 C. 1st cycle (——), 2nd cycle (•••••), 3rd cycle (· · ·), 5th cycle (–•–•), 10th cycle (-----). b) Cycling performance and Coulombic efficiency of Se/CMK-3 with SA and PVDF binders (rate: 0.1 C). c) Reversible capability density of Se/CMK-3 at 0.1 C, 1 C, 2 C, and 5 C, and long cycling performance at 1 C.

major part of the initial capacity loss of the Se/CMK-3 cathode and also explains its higher capacity than the theoretical capacity of Se.

Figure 3b shows the comparison of the discharge capacities and Coulombic efficiencies of the Se/CMK-3 cathode with SA binder and with PVDF binder. For the Se/CMK-3 cathode with SA binder, a reversible capacity of 600 (300) $mA\,h\,g^{-1}$ (2560 (630) $mA\,h\,cm^{-3}$) is obtained after 50 cycles, with the Coulombic efficiency always approaching 100%, thus confirming its excellent cyclability. The high Coulombic efficiency also indicates that the shuttle effect has been restrained in the Li–Se battery. To confirm the nonexistence of the shuttle effect in the Li–Se/CMK-3 battery, a battery was disassembled after 100 cycles for ex situ observation of the Li anode. As shown in Figure S3a, the cycled Li anode retains a smooth surface, and no Se was detected in the Li anode by EDX analysis. Ex situ X-ray photoelectron spectroscopic analysis (Figure S3b) further reveals that no Se is deposited on the surface of the Li anode after extended cycling, thus implying that the Li–Se/CMK-3 battery does not suffer from the shuttle effect.

Compared with the electrode with a SA binder, the Se/CMK-3 electrode with a PVDF binder exhibits similar electrochemical behavior, but inferior performance (Figures 3b and S4). Its irreversible capacity in the first cycle is very large; thus, the reversible capacity is lower (ca. 400 (200) $mA\,h\,g^{-1}$). Given that Se is slightly soluble in NMP, when the PVDF binder (dissolved in NMP) is used to paste the electrode, a small quantity of Se in the mesopores of CMK-3 will dissolve in NMP and precipitate as bulk crystalline Se outside the mesopores. Many dendritic crystals are observed on the electrode when PVDF is used as the binder (Figure S5a). Point EDX analysis (Figure S6) and element distribution mapping (Figure S7) imply that the dendritic crystals are likely bulk Se. The result is consistent with the XRD pattern (Figure S8), which further confirms the existence of trigonal Se on the electrode with the PVDF binder. The crystalline Se disappears after the first discharge (Figure S5b) and does not form in the subsequent cycles (Figures S5c and S8). Therefore, the bulk crystalline Se is responsible for the low active material utilization and the large initial capacity loss of the Se/CMK-3 cathode with PVDF binder. By contrast, no crystalline Se is observed on the Se/CMK-3 cathode with SA binder (Figure S5d). Thus, the Se/CMK-3 cathode with SA binder shows considerably improved capacity and Coulombic efficiency.

Figure 3c further supports the superior cycling stability and rate performance of the Se/CMK-3 cathode with SA binder. After activation at 0.1 C (67 $mA\,g^{-1}$ based on the mass of Se, same below), upon cycling under current densities of 1 C, 2 C, and 5 C, Se/CMK-3 reversibly delivers approximately 72%, 60%, and 46% of the theoretical capacity of Se, respectively. When the rate recovers to 1 C, the reversible capacity regains 64% of the theoretical capacity. Even after 500 cycles, 45% of the theoretical capacity is retained.

To find the effect of the Se content in the composite, the electrochemical performance of Se/CMK-3 with 70 wt% of Se (Se/CMK-3-70) was tested. Although the specific capacity of Se/CMK-3-70 is slightly lower than Se/CMK-3-50, Se/CMK-3-70 exhibits a similar discharge/charge performance with Se/CMK-3-50 (Figure S9). In addition, considering the high Se content, Se/CMK-3-70 delivers a high and stable volumetric capacity density of ca. 2200 (870) $mA\,h\,cm^{-3}$, which is retained after 30 cycles, thus supporting its feasibility for compact high-energy batteries.

As shown in Figure 3a, the electrochemical performance of Se/CMK-3 differs from that in a previous report,[8] where Se crystals were found in the cathode material. The electrochemical reaction mechanism of Se/CMK-3 is of great interest; therefore, the chemical constituents of the active material at different discharge/charge states were further investigated by ex situ XRD and Raman spectroscopy (Figure 4). Based on the ex situ analysis, a possible mechanism was proposed and is shown in Figure 5. The crystal structure of trigonal Se in Se-CMK-3 is maintained, as confirmed by the XRD pattern (Figure 2a) and the Raman shift at 233 cm^{-1} (Figure 4b), which is attributed to the first-order A_1 symmetric bond-stretching modes of trigonal Se.[11] After heating the Se-CMK-3 mixture, crystalline Se disappears and is converted into cyclic Se_8 molecules (Raman shift of 267 cm^{-1}) inside the mesopores of CMK-3. The process of pasting the electrode with SA binder has no considerable effect on the structure of Se, because the XRD and Raman signals of the electrode are the same as those of the composite. After the first discharge to 1.0 V, Se_8 reacts with Li to form Li_2Se, as confirmed by the XRD pattern. Unlike the reaction between Li^+ and bulk Se in the previous report,[8] Li^+ reacts directly with every single Se_8 molecule in the mesopores of CMK-3 to generate the final Li_2Se product,

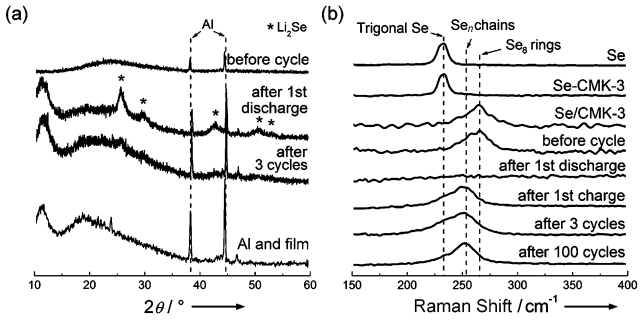

Figure 4. a) XRD patterns of the Se/CMK-3 cathode with SA binder before cycle, after the first discharge, and after 3 discharge/charge cycles. The base, consisting of Al foil and a film to separate the cathode from air and water, is also shown. b) Raman spectra of pristine Se, Se-CMK-3, Se/CMK-3, and the Se/CMK-3 cathode with SA binder before cycle, after the first discharge, after the first charge (1 discharge/charge cycle), after 3 discharge/charge cycles, and after 100 discharge/charge cycles.

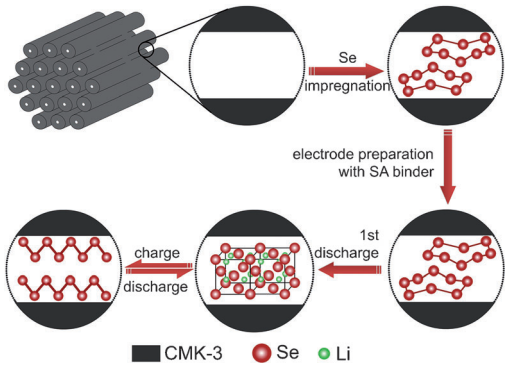

Figure 5. Proposed lithiation/delithiation processes of Se/CMK-3.

which is associated with the single-plateau discharge reaction. When charged, chain-like Se is formed instead of cyclic Se_8, which can be inferred from the Raman shift of the product at 256 cm^{-1}; this shift corresponds to the vibrations of amorphous Se comprised of disordered Se chains. The Se atoms in chain-like Se_n molecules have a stronger interaction with the C substrate than that in the Se_8 rings, in which Se–Se interaction is dominant. Therefore, the conversion results in Se molecules confined in the mesopores with improved stability. Thus, the shuttle effect, which encumbers the application of Li–S batteries, is avoided. In addition, the transformation between Se and Li_2Se is complete, as deduced from the nonappearance of Se–Se bond stretching in the Raman spectrum in the Li-insertion state, and the absence of Li_2Se in the XRD pattern in the Li-extraction state. Thus, Coulombic efficiency is almost 100%, except during the first cycle.

In conclusion, we have confined Se in the form of cyclic Se_8 molecules in ordered mesoporous carbon by a facile melt-diffusion route, and observed the conversion of the molecules from Se_8 rings into Se_n chains in the mesopores during electrochemical cycling. The Se molecules are stable because of the mesoporous confinement and the strong interaction between the chain-like Se_n molecules and the carbon substrate. Owing to this form of Se in the Se/CMK-3 composite, the composite exhibits single-plateau electrochemical behavior, excellent cycling stability, and good rate performance. We selected a water-soluble binder to further avoid the formation of bulk Se during electrode preparation. When pasted with the SA binder, the Se/CMK-3 cathode is able to deliver a high reversible discharge capacity of ca. 600 (300) mA h g^{-1} after 50 cycles. With the unique advantages of Se molecules confined in ordered mesoporous carbon matrixes, including high volumetric energy density, superior cycling performance, good conductivity, and reaction process without shuttle effect, they can be applied not only in Li batteries, but also in Na and Mg batteries, which will provide new candidates for high-performance rechargeable batteries.

Received: April 15, 2013
Revised: May 13, 2013
Published online: June 26, 2013

Keywords: carbon · cathode materials · lithium · mesoporous materials · selenium

[1] a) M. Armand, J.-M. Tarascon, *Nature* **2008**, *451*, 652–657; b) Y.-K. Sun, S.-T. Myung, B.-C. Park, J. Prakash, I. Belharouak, K. Amine, *Nat. Mater.* **2009**, *8*, 320–324; c) Y.-M. Chiang, *Science* **2010**, *330*, 1485–1486; d) J. B. Goodenough, Y. Kim, *Chem. Mater.* **2010**, *22*, 587–603; e) B. Scrosati, J. Garche, *J. Power Sources* **2010**, *195*, 2419–2430; f) J. Chen, F. Cheng, *Acc. Chem. Res.* **2009**, *42*, 713–723; g) L. Hu, H. Wu, F. La Mantia, Y. Yang, Y. Cui, *ACS Nano* **2010**, *4*, 5843–5848; h) Y. Wang, G. Cao, *Adv. Mater.* **2008**, *20*, 2251–2269; i) Y.-G. Guo, J.-S. Hu, L.-J. Wan, *Adv. Mater.* **2008**, *20*, 2878–2887; j) Y. Yu, L. Gu, C. Zhu, P. A. van Aken, J. Maier, *J. Am. Chem. Soc.* **2009**, *131*, 15984–15985; k) X. Meng, X. Q. Yang, X. Sun, *Adv. Mater.* **2012**, *24*, 3589–3615; l) T. Zhang, H. Zhou, *Angew. Chem.* **2012**, *124*, 11224–11229; *Angew. Chem. Int. Ed.* **2012**, *51*, 11062–11067; m) S. Xin, Y.-G. Guo, L.-J. Wan, *Acc. Chem. Res.* **2012**, *45*, 1759–1769; n) L. Wang, X. He, J. Li, W. Sun, J. Gao, J. Guo, C. Jiang, *Angew. Chem.* **2012**, *124*, 9168–9171; *Angew. Chem. Int. Ed.* **2012**, *51*, 9034–9037.

[2] a) X. Ji, L. F. Nazar, *J. Mater. Chem.* **2010**, *20*, 9821–9826; b) P. G. Bruce, S. A. Freunberger, L. J. Hardwick, J.-M. Tarascon, *Nat. Mater.* **2012**, *11*, 19–29; c) A. Manthiram, Y. Fu, Y.-S. Su, *Acc. Chem. Res.* **2013**, *46*, 1125–1134; d) S. Evers, L. F. Nazar, *Acc. Chem. Res.* **2013**, *46*, 1135–1143.

[3] a) S.-Y. Chung, J. T. Bloking, Y.-M. Chiang, *Nat. Mater.* **2002**, *1*, 123–128; b) S.-E. Cheon, K.-S. Ko, J.-H. Cho, S.-W. Kim, E.-Y. Chin, H.-T. Kim, *J. Electrochem. Soc.* **2003**, *150*, A796–A799.

[4] a) X. Ji, K. T. Lee, L. F. Nazar, *Nat. Mater.* **2009**, *8*, 500–506; b) N. Jayaprakash, J. Shen, S. S. Moganty, A. Corona, L. A. Archer, *Angew. Chem.* **2011**, *123*, 6026–6030; *Angew. Chem. Int. Ed.* **2011**, *50*, 5904–5908; c) S.-R. Chen, Y.-P. Zhai, G.-L. Xu, Y.-X. Jiang, D.-Y. Zhao, J.-T. Li, L. Huang, S.-G. Sun, *Electrochim. Acta* **2011**, *56*, 9549–9555; d) G. Zheng, Y. Yang, J. J. Cha, S. S. Hong, Y. Cui, *Nano Lett.* **2011**, *11*, 4462–4467; e) C. Zhang, H. B. Wu, C. Yuan, Z. Guo, X. W. D. Lou, *Angew. Chem.* **2012**, *124*, 9730–9733; *Angew. Chem. Int. Ed.* **2012**, *51*, 9592–9595; f) X. Li, Y. Cao, W. Qi, L. V. Saraf, J. Xiao, Z. Nie, J. Mietek, J.-G. Zhang, B. Schwenzer, J. Liu, *J. Mater. Chem.* **2011**, *21*, 16603–16610; g) S. Xin, L. Gu, N. H. Zhao, Y. X. Yin, L. J. Zhou, Y.-G. Guo, L. J. Wan, *J. Am. Chem. Soc.* **2012**, *134*, 18510–18513; h) H. Ye, Y.-X. Yin, S. Xin, Y.-G. Guo, *J. Mater. Chem. A* **2013**, *1*, 6602–6608; i) L. Ji, M. Rao, H. Zheng, L. Zhang, Y. Li, W. Duan, J. Guo, E. J. Cairns, Y. Zhang, *J. Am. Chem. Soc.* **2011**, *133*, 18522–18525; j) Y. Yang, G. Yu, J. J. Cha, H. Wu, M. Vosguer-

itchian, Y. Yao, Z. Bao, Y. Cui, *Acs Nano* **2011**, *5*, 9187 – 9193; k) J. Guo, Y. Xu, C. Wang, *Nano Lett.* **2011**, *11*, 4288 – 4294; l) R. Demir-Cakan, M. Morcrette, F. Nouar, C. Davoisne, T. Devic, D. Gonbeau, R. Dominko, C. Serre, G. Ferey, J. M. Tarascon, *J. Am. Chem. Soc.* **2011**, *133*, 16154 – 16160; m) J. Kim, D.-J. Lee, H.-G. Jung, Y.-K. Sun, J. Hassoun, B. Scrosati, *Adv. Funct. Mater.* **2013**, *23*, 1076 – 1080.

[5] a) F. Wu, J. Chen, R. Chen, S. Wu, L. Li, S. Chen, T. Zhao, *J. Phys. Chem. C* **2011**, *115*, 6057 – 6063; b) Z. W. Seh, W. Li, J. J. Cha, G. Zheng, Y. Yang, M. T. McDowell, P.-C. Hsu, Y. Cui, *Nat. Commun.* **2013**, *4*, 1331 – 1336.

[6] a) D.-R. Chang, S.-H. Lee, S.-W. Kim, H.-T. Kim, *J. Power Sources* **2002**, *112*, 452 – 460; b) J. Wang, S. Y. Chew, Z. W. Zhao, S. Ashraf, D. Wexler, J. Chen, S. H. Ng, S. L. Chou, H. K. Liu, *Carbon* **2008**, *46*, 229 – 235; c) L. Suo, Y. S. Hu, H. Li, M. Armand, L. Chen, *Nat. Commun.* **2013**, *4*, 1481 – 1489.

[7] X. Liang, Z. Wen, Y. Liu, M. Wu, J. Jin, H. Zhang, X. Wu, *J. Power Sources* **2011**, *196*, 9839 – 9843.

[8] A. Abouimrane, D. Dambournet, K. W. Chapman, P. J. Chupas, W. Weng, K. Amine, *J. Am. Chem. Soc.* **2012**, *134*, 4505 – 4508.

[9] H. S. Kim, T. S. Arthur, G. D. Allred, J. Zajicek, J. G. Newman, A. E. Rodnyansky, A. G. Oliver, W. C. Boggess, J. Muldoon, *Nat. Commun.* **2011**, *2*, 427 – 432.

[10] I. Kovalenko, B. Zdyrko, A. Magasinski, B. Hertzberg, Z. Milicev, R. Burtovyy, I. Luzinov, G. Yushin, *Science* **2011**, *334*, 75 – 79.

[11] a) I. L. Li, J. P. Zhai, P. Launois, S. C. Ruan, Z. K. Tang, *J. Am. Chem. Soc.* **2005**, *127*, 16111 – 16119; b) I. L. Li, S. C. Ruan, Z. M. Li, J. P. Zhai, Z. K. Tang, *Appl. Phys. Lett.* **2005**, *87*, 071902.

